Article:
McDermott, M, Resende, PR, Wilson, MCT orcid.org/0000-0002-1058-2003 et al. (3 more authors) (2021) An improved k - ω turbulence model for FENE-P fluids without friction velocity dependence. International Journal of Heat and Fluid Flow, 90. 108799. ISSN 0142-727X

https://doi.org/10.1016/j.ijheatfluidflow.2021.108799

An improved $k-\omega$ turbulence model for FENE-P fluids without friction velocity dependence

M. McDermott[a], P.R. Resende[b], M.C.T. Wilson[a], A.M. Afonso[c], D. Harbottle[d], G. de Boer[a]

[a] *School of Mechanical Engineering, University of Leeds, 191 Woodhouse Ln, Leeds LS2 9JT, UK*

[b] *ProMetheus, Escola Superior de Tecnologia e Gestão, Instituto Politécnico de Viana do Castelo, 4900-347 Viana do Castelo, Portugal*

[c] *Transport Phenomena Research Center, Faculty of Engineering, University of Porto, Rua Dr. Roberto Frais s/n, 4200-465 Porto, Portugal*

[d] *School of Chemical and Process Engineering, University of Leeds, 211 Clarendon Rd, Leeds LS2 9JT, UK*

Abstract

An improved $k-\omega$ turbulence model for viscoelastic fluids is developed to predict turbulent flows, with polymeric solutions described by the finitely extensible nonlinear elastic-Peterlin constitutive model. The $k-\omega$ model is tested against a wide range of direct numerical simulation data in fully-developed channel flow, with different rheological parameter combinations, and can predict all regimes of drag reduction (low, intermediate and high) with good performance. Closures are improved for the NLT_{ij} term, which captures the polymer extension due to turbulent fluctuations; a modified damping function, f_μ, which accounts for the turbulent kinetic energy re-distribution process; and the viscoelastic destruction term, E_{τ_p}. The main

Email addresses: ed11m22m@leeds.ac.uk (M. McDermott), pedroresende@estg.ipvc.pt (P.R. Resende), M.Wilson@leeds.ac.uk (M.C.T. Wilson), aafonso@fe.up.pt (A.M. Afonso), D.Harbottle@leeds.ac.uk (D. Harbottle), G.N.deBoer@leeds.ac.uk (G. de Boer)

advantage of the current model is its ability to predict all flow features with model simplicity and without the need for friction velocity dependence, important for flows with reattachment due to their singularity caused by the stagnation points.

Keywords: Drag reduction, FENE-P fluid, Viscoelastic RANS model, OpenFoam CFD.

1. Introduction

Predicting the behaviour of turbulent flows containing drag reducing polymer additives has been an active area of research since the experimental discovery of Toms et al. [1], who demonstrated that dilute solutions of flexible high-molecular weight polymers can drastically reduce the transport energy in channel flows by upto 80%. Virk [2] quantified many early experimental studies and proposed a maximum drag reduction (MDR) limit, in which the polymer chains cannot further relaminarise the turbulent structures. Comprehensive studies followed to understand the mechanisms and interactions between the polymer chains and turbulent structures: Lumley [3] suggesting that the drag reduction (DR) phenomenon is caused by an *effective viscosity* outside the viscous layer, whilst the elastic explanation of Tabor & De Gennes [4] states that polymers inhibit the turbulent energy transfer during coil-stretch transition, extending the buffer layer.

Several direct numerical simulation (DNS) investigations were carried out with various rheological models [5; 6; 7; 8] to understand the complex interactions between the polymer chains and turbulent shears within channel flows, most notably with the FENE-P (finitely extensible nonlinear elastic-Peterlin)

dumb-bell constitutive model because of its molecular roots in kinetic theory [9; 10]. The FENE-P model can predict the effects on turbulent shear stresses via the polymer relaxation time, polymer chain extensibility and the polymer/solvent viscosity ratio. It is now known that drag reduction is strongly associated with the suppression of near-wall turbulent vortical dynamics by the extensional motion of the polymer chains [11], inducing a redistribution of the turbulent energy scales and a global reduction in mean eddy structures.

The abundance of DNS data [12; 13; 14; 15; 8] for Reynolds-averaged quantities in fully-developed channel flow allows for the development of closure models, which substantially reduces the high CPU resource demands associated with the grid resolution required to capture near-wall elongated velocity streaks. This is ideal for engineering pursuits, and consequently Reynolds-Averaged-Navier-Stokes (RANS) turbulent viscoelastic models have been developed in order to capture important mean flow properties.

First attempts to incorporate the viscoelastic rheology of drag reducing fluids within turbulence models came from the group of Pinho and co-workers [16; 17; 18; 19; 20], who adopted a Generalised Newtonian Fluid (GNF) constitutive equation and modified it to incorporate the elastic contribution by involving dependency of the fluid strain hardening on the third invariant of the rate of deformation tensor. However, GNF models are not true viscoelastic constitutive models as they only account for inelastic effects.

The first elastic model was developed by Leighton et al. [21], based on the FENE-P dumbbell constitutive equation model. Their study involved the development of a polymer strain-stress coupling based on the tensor expansion, which incorporated the conformation tensor and Reynolds stress. Pinho et al.

[22] extended the Newtonian $k-\varepsilon$ low-Reynolds number turbulence model of Nagano et al. [23; 24] by introducing new turbulent viscoelastic closures including: the non-linear term involving the conformation tensor and the strain rate fluctuations within the conformation tensor equation (denoted NLT_{ij} following the nomenclature of Housiadas et al. [25] and Li et al. [26]); along with the viscoelastic turbulent transport terms of the turbulent kinetic energy. The model could predict low drag reduction (LDR) features, but failed to capture the increase of turbulent kinetic energy for increasing viscoelasticty as suggested by the DNS findings [13]. Subsequently, Resende et al. [27] improved the model upto intermediate drag reduction (IDR) by developing closures for the NLT_{ij} term, and introducing a polymer contribution to the eddy viscosity closure model. Nonetheless, the model still under-predicted the turbulent kinetic energy with increasing DR, and featured an exceedingly complex closure for NLT_{ij} with many damping functions and model coefficients. The same closures were later applied by Resende et al. [28] to the Newtonian $k-\omega$ model of Bredberg et al. [29], via a mathematical transformation of the governing terms involving ω, and the turbulent-viscoelastic correlations. The closures had identical limitations as the $k-\varepsilon$ model for predicting DR behaviour, but demonstrated great versatility and robustness given its application to alternative two-equation models.

Iaccarino et al. [30] proposed a $k-\varepsilon-v^2-f$ model for FENE-P fluids in fully developed channel flow, extending the Newtonian model of Durbin et al. [31]. In the v^2-f model approach, the eddy viscosity depends on a scalar turbulent velocity scale which incorporates near-wall turbulence anisotropy as well as non-local pressure strain effects. In their model [30], they introduce

the concept of a *turbulent polymer viscosity* which accounts for the combined effect of viscoelasticity and turbulence on the polymer stress in the momentum equation. The closures developed for NLT_{ij} are much simpler than those developed by Resende et al. [27] for the $k-\varepsilon$ isotropic model, but depend only on the trace of the conformation tensor and not the individual components. The NLT_{yy} component is the dominant contributor to the transverse conformation tensor component (C_{yy}) and an *effective polymer viscosity* [32], meaning the additional anisotropic closures for v^2 are forced *ad hoc*.

Masoudian et al. [15] later improved the $k-\varepsilon-v^2-f$ model and predicted flow features upto HDR. The key advancements were a result of the new NLT_{ij} closure being made proportional to the local eddy viscosity based upon DNS analysis, and an *ad hoc* closure model for the viscoelastic turbulent cross-correlation in the v^2 equation. This model was improved further by Masoudian et al. [33] via slight adjustments to the aforementioned closures, along with adding a simple extension to include heat transfer. However, the model fails to capture the crucial NLT_{yy} component (zero in their model) and has an opposite sign for the NLT_{xy} component, which is contrary to the DNS analysis of the momentum balance in the polymer shear stress. Furthermore, the dissipation rate shows an opposite trend for increasing DR. A Reynolds Stress Model was also developed by Masoudian et al. [34] based upon the Newtonian model of Lai et al. [35], which was previously used by Resende et al. [20] to predict viscoelastic flows for a constitutive GNF model. In that work, the correlation between the Reynolds stresses and the NLT_{ij} components was generalised ($NLT_{ij} \sim \overline{u_i' u_j'}$). However, the model required an additional damping function and further friction velocity dependence for the

NLT_{ij} closure. The model can predict flow behaviour for a reasonable range of rheological properties, but largely under-predicts the turbulent kinetic energy magnitude by not capturing the increase of stream-wise turbulence for high DR (HDR) observed in the DNS studies [13].

Most recently, Resende et al. [36] improved upon the $k-\varepsilon$ model [27] via a modified damping function able to predict the turbulent redistribution process and thickening of the buffer layer. The correct increase of the turbulent kinetic energy was the first of the model's kind, achieved by analysing the production term behaviour near the wall [37], and by developing new eddy viscosity and NLT_{ij} closures using strictly DNS data [38]. In their work [36], they also improved significantly on the NLT_{ij} closure and incorporated small concentration variation via the solvent ratio. The model can predict most ranges of DR well, but still requires complex un-physical modelling containing bulk Reynolds number and friction velocity dependence. This occurs predominately within the NLT_{xx} term which accounts for the dominant stretch of polymer chains from turbulent shear stresses, which fails at higher Reynolds numbers. These limitations are addressed in the context of a $k-\varepsilon$ model [39], with the model predicting a larger range of DR behaviour, but without concentration variation.

Earlier proposals of a modified damping function came from Pinho et al. [16] with a GNF model for FENE-P fluids; and Tsukahara et al. [40] with a Giesekus model. In the latter study, the turbulent kinetic energy was largely over-predicted which was compensated for by a lack of closure for the viscoelastic destruction term within the ε transport equation. In some instances, the model demonstrated instabilities, predicting a 1% DR for a

DNS result of 23% DR.

In the present study, a $k-\omega$ model is developed based on the recent $k-\varepsilon$ model of McDermott et al. [39] and Resende et al. [36]. The model here introduces β variation, along with a new formulation of the damping function from the Newtonian model [29], which was designed to capture features in complex geometry such as the backwards facing step. The model vastly improves on the previous $k-\omega$ model of Resende et al. [28; 36]. The shortcomings in the model complexity of the NLT_{ij} term and other viscoelastic turbulent closures are addressed by applying a more physically based approach, and removing all additional damping functions and friction velocity dependence. An additional closure for the modified damping function is also proposed, capable of predicting the decrease of the eddy viscosity for all ranges of DR. The advantage of the current model is the ability to predict DR behaviour for a large range of flow and rheological parameters, with model simplicity and without the need for friction velocity dependence. This is advantageous for flows with reattachment such as the backward facing step, which is the key feature of the Newtonian model this work is derived from.

The paper is organised as follows: Section 2 introduces the instantaneous and time-averaged governing equations and identifies some of viscoelastic terms that will require modelling; Section 3 introduces the closures to the Newtonian turbulence model and changes to the damping function, along with presenting the other viscoelastic terms that need closures; Section 4 explains in detail the development of the viscoelastic turbulent closures based on comparisons with DNS data of fully developed channel flow present within

the literature; Section 5 summarises the model; Section 6 presents the results of the flow fields in fully developed channel flow, covering all ranges of DR and flow conditions; and finally in Section 7, the main conclusions are presented.

2. Governing Equations

The exact instantaneous continuity and momentum equations for the turbulent flow of incompressible dilute polymer solution, where the rheological properties are based on the FENE-P constitutive model [10], are:

$$\frac{\partial \hat{u}_k}{\partial x_k} = 0, \tag{1}$$

$$\rho\left(\frac{\partial \hat{u}_i}{\partial t} + \hat{u}_k \frac{\partial \hat{u}_i}{\partial x_k}\right) = -\frac{\partial \hat{p}}{\partial x_i} + \frac{\partial \hat{\tau}_{ik}}{\partial x_k}, \tag{2}$$

where the hat represents instantaneous quantities of velocity $\hat{u}_i$, pressure $\hat{p}$, stress tensor $\hat{\tau}_{ik}$, and fluid density ρ. The stress tensor is the sum of the Newtonian solvent which obeys Newton's law of viscosity, $\hat{\tau}^s_{ik} = 2\mu_s \hat{s}_{ij}$, with μ_s representing the solvent viscosity coefficient, and polymeric contributions, $\hat{\tau}^p_{ik}$,

$$\hat{\tau}_{ik} = \hat{\tau}^s_{ik} + \hat{\tau}^p_{ik}. \tag{3}$$

The instantaneous rate of strain tensor, $\hat{s}_{ij}$, is defined as

$$\hat{s}_{ij} = \frac{1}{2}\left(\frac{\partial \hat{u}_i}{\partial x_j} + \frac{\partial \hat{u}_j}{\partial x_i}\right). \tag{4}$$

The definition of the instantaneous polymer stresses based on the FENE-P closure is given by Eq. (5) and Eq. (6) as a function of the instantaneous conformation tensor $\hat{c}_{ij}$.

$$\hat{\tau}^p_{ij} = \frac{\mu_p}{\lambda}\left(f(\hat{c}_{kk})\hat{c}_{ij} - f(L)\delta_{ij}\right) \tag{5}$$

with Peterlin function

$$f(\hat{c}_{kk}) = \frac{L^2 - 3}{L^2 - \hat{c}_{kk}} \quad \text{and} \quad f(L) = 1, \tag{6}$$

where δ_{ij} is the Kronecker delta function and $f(L)\delta_{ij}$ represents the limit on the Peterlin function for the equilibrium point of the dumbbell model. $\hat{c}_{kk}$ is the trace of the instantaneous conformation tensor, and the other parameters are associated to the rheological model: L^2 denotes the maximum molecular extensibility of the model dumbbell; λ is the relaxation time of the fluid and μ_p is the polymer viscosity coefficient. The conformation tensor behaviour obeys the following hyperbolic differential equation

$$\frac{\partial \hat{c}_{ij}}{\partial t} + \hat{u}_k \frac{\partial \hat{c}_{ij}}{\partial x_k} - \left(\hat{c}_{kj} \frac{\partial \hat{u}_i}{\partial x_k} + \hat{c}_{ik} \frac{\partial \hat{u}_j}{\partial x_k} \right) = \overset{\nabla}{\hat{c}}_{ij} = -\frac{\hat{\tau}^p_{ij}}{\mu_p}. \tag{7}$$

The $\overset{\nabla}{\hat{c}}_{ij}$ term denotes Oldroyd's upper convective derivative of the instantaneous conformation tensor. The first two terms are the material derivative and represent the local and advective derivatives, and the terms in brackets account for the polymer stretching by the instantaneous flow.

The Reynolds averaged equations can be obtained by applying the Reynolds decomposition to the instantaneous quantity, $\hat{u}_i = U_i + u_i$, where upper-case letters or overbars represent average/mean quantities and lower-case letters or primes represent fluctuating quantities. The Reynolds averaged Navier-Stokes (RANS) equations are given by:

$$\frac{\partial U_k}{\partial x_k} = 0, \tag{8}$$

$$\rho \frac{\partial U_i}{\partial t} + \rho U_k \frac{\partial U_i}{\partial x_k} = -\frac{\partial \overline{p}}{\partial x_i} + \mu_s \frac{\partial^2 U_i}{\partial x_k \partial x_k} - \frac{\partial}{\partial x_k}(\rho \overline{u_i u_k}) + \frac{\partial \overline{\tau}^p_{ik}}{\partial x_k}, \tag{9}$$

where $\overline{p}$ is the mean pressure, U_i is the mean velocity, $-\rho\overline{u_i u_k}$ is the Reynolds stress tensor and $\overline{\tau}^p_{ik}$ is the Reynolds-averaged polymer stress, taking the form

$$\overline{\tau}^p_{ij} = \frac{\mu_p}{\lambda}\left[\overline{f(C_{kk}+c_{kk})(C_{ij}+c_{ij})} - f(L)\delta_{ij}\right]. \tag{10}$$

The mean conformation tensor, C_{ij}, is determined by the Reynolds-averaged Conformation Evolution (RACE):

$$\frac{DC_{ij}}{Dt} - M_{ij} + CT_{ij} - NLT_{ij} = \frac{\overline{\tau}^p_{ij}}{\mu_p}, \tag{11}$$

$$M_{ij} = C_{jk}\frac{\partial U_i}{\partial x_k} + C_{ik}\frac{\partial U_j}{\partial x_k}, \tag{12}$$

$$CT_{ij} = \overline{u_k \frac{\partial c_{ij}}{\partial x_k}}, \tag{13}$$

$$NLT_{ij} = \overline{c_{jk}\frac{\partial u_i}{\partial x_k}} + \overline{c_{ik}\frac{\partial u_j}{\partial x_k}}, \tag{14}$$

where M_{ij}, the mean flow distortion term, is non-zero, but requires no closure. The remaining two terms are related to turbulent correlations and, following the analysis and nomenclature of Li et al. [26] and Housiadas et al. [25] are labelled with CT_{ij}, representing the contribution to the transport of the conformation tensor due to the fluctuating advective terms, and NLT_{ij} which accounts for the interactions between the fluctuating components of the conformation tensor and the velocity gradient tensor. A contribution comparison was made to the terms of the average conformation tensor equation, Eq. (11), and confirmed that the CT_{ij} term can be neglected for all regimes of DR, in agreement with the finding of Housiadas et al. [25] and Li et al. [26]. However, the NLT_{ij} term cannot be neglected since it is a significant contribution and therefore requires a suitable closure.

3. Turbulence Model

The Reynolds stress tensor is computed by adopting the Boussinesq turbulent stress strain relationship,

$$-\rho\overline{u_i u_j} = 2\rho\nu_T S_{ij} - \frac{2}{3}\rho k\delta_{ij}, \tag{15}$$

where k is the turbulent kinetic energy, S_{ij} is the mean rate of strain tensor and ν_T is the eddy viscosity. ν_T is modelled by the typical isotropic $k-\omega$ turbulence model, which includes a damping function f_μ to account for near-wall effects,

$$\nu_T = f_\mu \frac{k}{\omega}, \tag{16}$$

where ω is the specific rate of dissipation of k. The $k-\omega$ Newtonian transport equations are represented by the Bredberg model [29] which is presented further but with an alternative representation of f_μ. In their work, the damping function was derived from semi-empirical data and the final form is given as,

$$f_\mu^{\text{Bredberg}} = 0.09 + \left(0.91 + \frac{1}{R_t^3}\right)\left[1 - \exp\left\{-\left(\frac{R_t}{25}\right)^{2.75}\right\}\right], \tag{17}$$

with $R_t = k/(\nu_s\omega^N)$. The alternative formulation is based on the Newtonian model of Nagano et al. [23] [24] which employs a Van-Driest type damping function of the form,

$$f_\mu^{\text{Nagano}} = \left[1 - \exp\left(-\frac{y^+}{26.5}\right)\right]^2, \tag{18}$$

where $y^+ = u_{\tau_0} y/\nu_0$ is the dimensionless wall scaling, u_{τ_0} is the friction velocity, y is the distance to the nearest wall, and ν_0 is the sum of solvent and polymer viscosity coefficients ($\nu_0 = \nu_s + \nu_p$).

An adjustment is made to our model to remove the friction velocity dependence by using an alternative representation of y^+, with the near-wall scaling, y^*, motivated by Wallin et al. [41] such that,

$$y^* = C_{y1} Re_y^{1/2} + C_{y2} Re_y^2, \tag{19}$$

where $Re_y \equiv \sqrt{k} y/\nu_0$, with $C_{y1} = 2.2$ and $C_{y2} = 0.003$. The model constants are slightly adjusted from [41] as they apply a damping function of power 1. The final form of our Newtonian damping function model is given by,

$$f_\mu = \left[1 - \exp\left(-\frac{y^*}{a_\mu}\right)\right]^2, \tag{20}$$

with $a_\mu = 26.5$ and y^* given as Eq. (19). The damping function requires further modelling to include viscoelastic effects of the drag reducing flow, to be discussed further in the study.

The governing transport equation for the turbulent kinetic energy for turbulent FENE-P fluids was initially developed by [28], and is given by,

$$\begin{aligned}\rho\frac{\partial k}{\partial t} + \rho U_i \frac{\partial k}{\partial x_i} =& \frac{\partial}{\partial x_i}\left[\left(\mu_\mathrm{s} + \frac{\rho\nu_\mathrm{T}}{\sigma_k}\right)\frac{\partial k}{\partial x_i}\right] + P_k - \rho C_\mu \omega k \\ &+ Q^V - \rho\varepsilon^V,\end{aligned} \tag{21}$$

where $P_k = -\rho\overline{u_i u_j}\frac{\partial U_i}{\partial x_j}$ is the rate of production of k, and $\sigma_k = 1.0$. The last two terms on the right side of Eq. (21) are:

$$Q^V = \frac{\partial\overline{\tau'_{ik,p} u_i}}{\partial x_k} \quad \text{and} \quad \varepsilon^V = \frac{1}{\rho}\overline{\tau'_{ik,p}\frac{\partial u_i}{\partial x_k}}, \tag{22}$$

which are the viscoelastic turbulent transport and the viscoelastic stress work, respectively. They represent the fluctuating viscoelastic turbulent part of the k transport equation and require suitable closure models.

A budget analysis for each term in the k transport equation was performed by Pinho et al. [22] for different regimes of DR. They demonstrated that the magnitude of Q^V has more impact on the overall budget in the IDR, and also developed a closure. In the HDR, the amplitude of Q^V is the same as ε^V but has a different location in the buffer layer, in which the effects of Q^V are overcome by the turbulent diffusion, thus revealing negligible effects to overall flow predictions. Masoudian et al. [15] and Resende et al. [36] chose to neglect the Q^V contribution and this is also ignored here. However, ε^V cannot be neglected and a suitable closure model is required.

The corresponding transport equation for the specific rate of dissipation, ω, in turbulent channel flow for FENE-P fluids is defined by,

$$\rho\frac{\partial\omega}{\partial t}+\rho U_i\frac{\partial\omega}{\partial x_i}=\frac{\partial}{\partial x_i}\left[\left(\mu_{\rm s}+\frac{\rho\nu_{\rm T}}{\sigma_\omega}\right)\frac{\partial\omega}{\partial x_i}\right]+C_{\omega_1}\frac{\omega}{k}P_k-C_{\omega_2}\rho\omega^2 + \frac{C_\omega}{k}(\nu_s+\nu_T)\frac{\partial k}{\partial x_i}\frac{\partial\omega}{\partial x_i}+E_{\tau_{\rm p}}, \tag{23}$$

where $C_\omega = 0.9$, $C_{\omega1} = 0.49$, $C_{\omega2} = 0.072$ and $\sigma_\omega = 1.8$. The last term of Eq. (23) is the viscoelastic contribution to the ω transport and is given by,

$$E_{\tau_p}=\frac{2\mu_s\mu_p}{\lambda(L^2-3)}\overline{\frac{\partial u_i}{\partial x_m}\frac{\partial}{\partial x_k}\left\{\frac{\partial}{\partial x_m}[f(C_{nn})f(\hat{C}_{pp})c_{qq}C_{ik}]\right\}}. \tag{24}$$

It has non-negligible effects on flow predictions for all DR regimes and thus requires a suitable closure model. The full details of these equations can be found in Pinho et al. [22] and Resende et al. [28].

The performance of the Newtonian model and the effect of the damping function (Eq. (20)) with y^* (Eq. (19)) is analysed in Fig. 1 for fully developed turbulent channel flow at different friction Reynolds number regimes, $Re_{\tau_0} = 180, 395$ and 590. The correspondence between y^* and y^+ is good for $y^+ <$

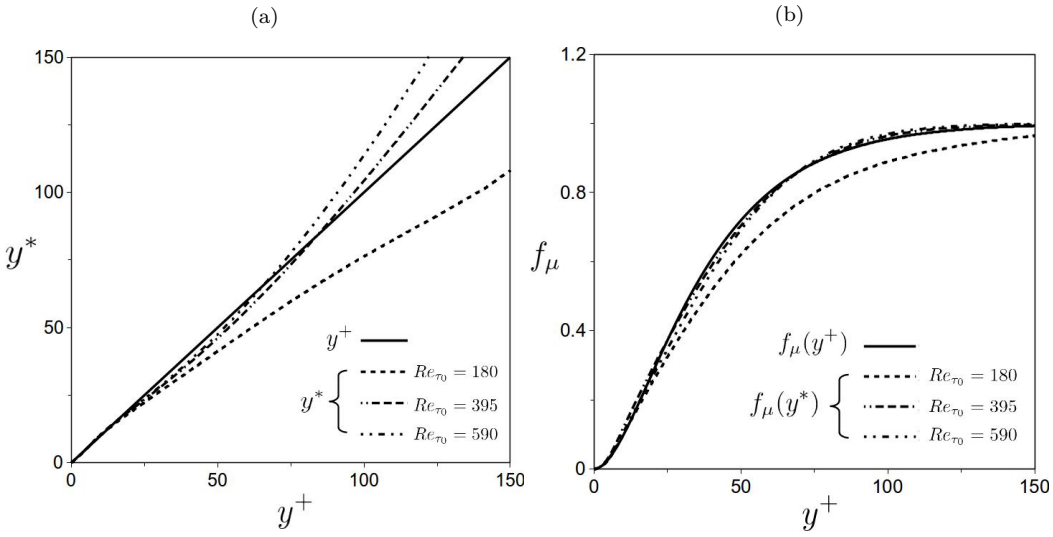

Figure 1: (a) Near-wall scaling comparison between y^+ (solid line) and y^* (Eq. 19) (dashed lines). (b) The damping function (Eq. 18) compared with Eq. 20 in Newtonian turbulent channel flow at $Re_{\tau_0} = 180, 395$ and 590.

100, with deviations at the lower Reynolds numbers (Fig. 1a). The damping function can be viewed in Fig. 1b where the deviations at $Re_{\tau_0} = 180$ are not sufficient to have a significant impact on model predictions, with higher Reynolds numbers showing excellent agreement. The mean streamwise velocity profile can be viewed in Fig. 2, predicting low, intermediate and high Reynolds number behaviour very well.

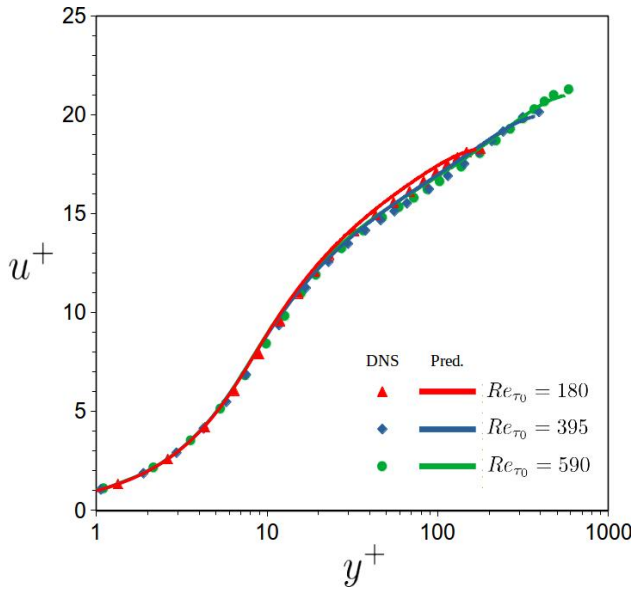

Figure 2: Comparison of the velocity profiles for Newtonian turbulent channel flow at $Re_{\tau_0} = 180, 395$ and 590 with DNS data [42] (symbols) and model predictions (solid lines).

4. Development of viscoelastic closures

In this section, closure models are developed for the turbulent viscoelastic cross-correlations, namely: NLT_{ij} (Eq. (14)); ε^V (Eq. (22)); E_{τ_p} (Eq. (24)) and a modified damping function, f_μ (Eq. (20)). The closure model predictions are validated against DNS data of fully developed channel flow at an intermediate friction Reynolds number of $Re_{\tau_0} = 395$ with a range rheological parameters, then subsequently compared to other DNS data sets for accurate turbulence modelling. The DNS data pertains to a large collection of studies (Table 1) in fully developed channel flow performed by Li et al. [13], Thais et al. [43], Masoudian et al. [15; 33; 44], Iaccarino et al. [30] and Ptasinski et al. [14].

Case	**Reference**	**Rheological parameters**				**Drag reduction (%)**	
		$Re_{\tau_0} = \frac{hu_\tau}{\nu_0}$	$\beta = \frac{\nu_s}{\nu_0}$	$Wi_{\tau_0} = \frac{\lambda u_\tau^2}{\nu_0}$	L^2	DNS	Model
(1)	Li et al. [13]	125	0.9	25	900	19	19
(2)	Li et al. [13]	125	0.9	25	3600	22	23
(3)	Li et al. [13]	125	0.9	50	1800	35	33
(4)	Li et al. [13]	125	0.9	100	900	37	34
(5)	Li et al. [13]	125	0.9	100	3600	56	49
(6)	Masoudian et al. [15]	180	0.9	25	900	19	20
(7)	Li et al. [13]	180	0.9	50	900	31	28
(8)	Masoudian et al. [15]	180	0.9	100	900	38	34
(9)	Masoudian et al. [15]	180	0.9	100	3600	54	47
(10)	Thais et al. [43]	180	0.9	116	10000	64	58
(11)	Iaccarino et al. [30]	300	0.9	36	3600	33	33
(12)	Iaccarino et al. [30]	300	0.9	120	10,000	59	59
(13)	Masoudian et al. [33]	395	0.9	25	900	19	23
(14)	Masoudian et al. [33]	395	0.9	50	900	30	30
(15)	Masoudian et al. [33]	395	0.9	50	3600	38	39
(16)	Masoudian et al. [33]	395	0.9	100	900	37	35
(17)	Masoudian et al. [33]	395	0.9	100	3600	48	48
(18)	Masoudian et al. [44]	395	0.9	100	10000	55	58
(19)	Masoudian et al. [33]	395	0.9	100	14,400	63	63
(20)	Thais et al. [43]	395	0.9	116	10,000	62	60
(21)	Li et al. [13]	395	0.9	200	14,400	75	70
(22)	Masoudian et al. [33]	590	0.9	50	3600	39	39
(23)	Thais et al. [43]	590	0.9	116	10,000	61	61
(A)	Ptasinski et al. [14]	180	0.8	54	1000	40	40
(B)	Ptasinski et al. [14]	180	0.6	54	1000	61	63
(C)	Ptasinski et al. [14]	180	0.6	72	1000	66	65

Table 1: Independent DNS data of fully-developed turbulent channel flow for FENE-P fluids with DR model predictions.

4.1. Closures for the conformation tensor

The first term that needs a closure is the mean polymer stress, Eq. (10). The expansion of this term can be written in the form,

$$\overline{\tau}^p_{ij} = \frac{\mu_p}{\lambda}\left[f(C_{kk})C_{ij} - f(L)\delta_{ij}\right] + \frac{\mu_p}{\lambda}\left[\overline{f(C_{kk}+c_{kk})(C_{ij}+c_{ij})} - f(C_{kk})C_{ij}\right]. \tag{25}$$

The magnitude of both terms on the RHS of Eq. (25) were analysed a priori using DNS data by [22]. They showed that at different values of L^2 and Wi_{τ_0}, the first term is nearly 20 times larger regardless of the rheological parameters. In this work, the mean polymer stress is approximated by the first term as with other models [30; 15; 33; 28], hence given by

$$\overline{\tau}^p_{ij} = \frac{\mu_p}{\lambda}\left[f(C_{kk})C_{ij} - f(L)\delta_{ij}\right]. \tag{26}$$

To compute the polymer stress, we need to calculate the components of the conformation tensor, C_{ij}, which are computed with the RACE (Eq. (11)). The set of analytical equations for fully developed channel flow can be viewed in Appendix 1 of [22]. The polymer shear stress component can be written as

$$\overline{\tau}^p_{xy} = \frac{\nu_p}{\lambda} f(C_{kk})C_{xy} = \nu_p \underbrace{\left(\frac{\lambda NLT_{yy}+1}{f(C_{mm})}\right)}_{C_{yy}} \frac{\mathrm{d}U}{\mathrm{d}y} + \nu_p NLT_{xy}. \tag{27}$$

In order to obtain predictions for the polymer shear stress in fully developed channel flow, one requires a closure model for C_{xy} and C_{kk}. The NLT_{yy} and NLT_{xy} terms act towards an effective polymer viscosity [32; 30]. The stretching of the polymer chains is accounted for by NLT_{kk}, and predominantly occur in the direction of mean flow or direction of the largest normal Reynolds stress, xx.

Here, a closure is developed for all relevant components based on the $k-\varepsilon$ model of Resende et al. [36]. The NLT_{ij} closure is presented below in three key parts, with a detailed explanation of each term:

$$NLT_{ij} \approx \underbrace{f_N C_{N1} C_\mu \frac{\lambda\sqrt{L}k\omega}{\nu_0 f(C_{mm})}\delta_{ij}}_{I} - \underbrace{f_N^{1/4} C_{N2} M_{ij}}_{II} + \underbrace{C_{N3}\frac{k}{\nu_0}\sqrt{\frac{L(1-\beta)M_{nn}}{\gamma}}\frac{\frac{\partial U_i}{\partial x_k}\frac{\partial U_j}{\partial x_k}}{\gamma^2}}_{III}, \tag{28}$$

where $f_N = \nu_T/\nu_0$ is the local eddy viscosity, $\gamma = \sqrt{2S_{pq}S_{pq}}$ is the shear rate invariant, with model constants $C_{N1} = 0.02$, $C_{N2} = 0.3$ and $C_{N3} = 0.18$.

- Term I captures the NLT_{yy} component and is similar to the model found in Resende et al. [36]. The adjustments were made in the context of the $k-\omega$ model, with minor corrections to the parameter values.

- Term II is primarily responsible for capturing the shear component, NLT_{xy}, which is a key component in predicting C_{xy}. The correlation here is with the exact term, M_{ij} (see Eq. (12)), and by the local eddy viscosity, $f_N^{1/4}$. The $L^{0.15}$ variation is removed from the model developed by Resende et al. [36]. The negative part of the NLT_{xx} component is also captured here via the M_{xx} term, with this component acting as a destruction term near walls.

- Term III is developed to predict the NLT_{xx} component which is the dominant term in the trace of NLT_{ij}, responsible for the stretch of the polymer chains due to turbulent fluctuations. Following the same assumption as Masoudian et al. [34], one can see that $NLT_{xx} \sim \overline{u_x' u_x'} \sim k$. In physical terms, the turbulent stretching terms represent the ability of the turbulent fluctuations to act on the polymer chains. This stretching is effective if the

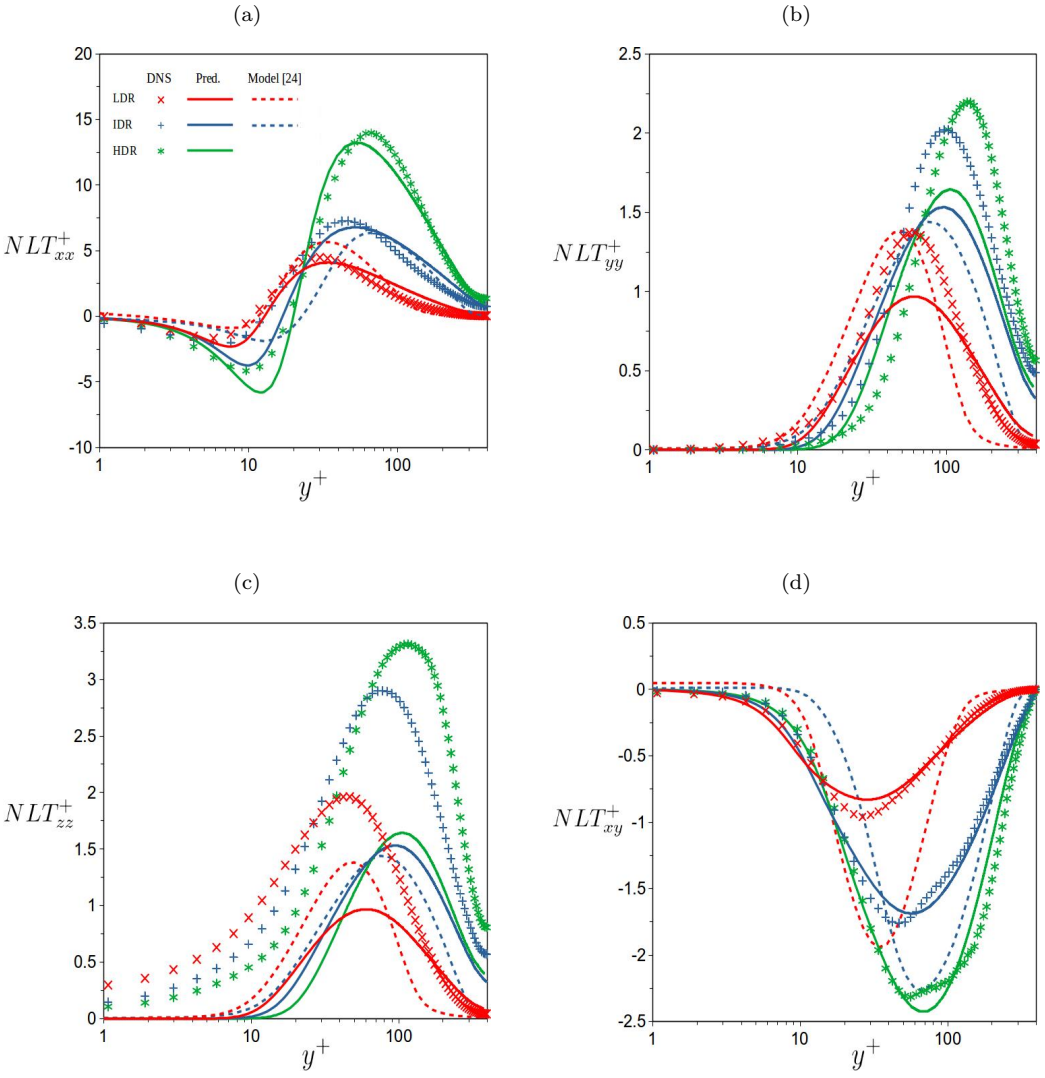

Figure 3: Comparison of the NLT_{ij} components between DNS data (symbols) and model predictions (lines) for channel flow at $Re_{\tau_0} = 395$: (a) NLT_{xx} (legend used for all figures); (b) NLT_{yy}; (c) NLT_{zz}; (d) NLT_{xy}. Each colour represents a different drag reduction regime: case 13 (LDR); case 16 (IDR); case 17 (HDR).

polymer shear, maximum extensibility and/or polymer concentration is large enough. So $\sqrt{L(1-\beta)M_{nn}/\gamma}$ is included here with k. Note that for fully developed channel flow, this term reduces to $\sqrt{L(1-\beta)C_{xy}}$ which increases proportional to drag reduction. This new term includes the same physical assumption as Masoudian et al [15; 33], and is simplified from the *ad hoc* approach of Resende et al. [36] which contained bulk parameters.

The performance of the individual components of NLT_{ij} can be analysed in Fig. 3 by comparing current model predictions against DNS data for low, intermediate and high DR in fully-developed turbulent channel flow at $Re_{\tau_0} = 395$. The previous $k-\omega$ model closure of NLT_{ij} from Resende et al. [28] can also be viewed comparatively here. Fig. 3a shows NLT_{xx}, the dominant polymer stretching term. It is clear that the model predictions match well with DNS data and improve significantly on the previous $k-\omega$ model of Resende et al. [28], requiring a much simpler closure without additional damping functions. Fig. 3b & 3d show the NLT_{yy} and NLT_{xy} terms respectively, needed for the polymer shear stress. The flow features are well captured such as the peak location and shift away from the wall for increasing viscoelasticity. Fig. 3c shows the NLT_{zz} component and generally under-predicts due to the isotropic assumption made between NLT_{yy} and NLT_{zz} based on term I in Eq. (28). Pinho et al. [22] showed that NLT_{zz} has low impact on flow features and thus the current model predictions are adequate for the purposes of this study. All flow features are well captured such as the magnitude and peak locations, improving significantly on the previous model. The effect of the NLT_{ij} closures on the mean conformation tensor are analysed in the results section.

4.2. Model for the modified damping function, f_μ

In viscoelastic turbulent flow, there is a reduction in the Reynolds shear stress and shift away from the wall as observed in the DNS [13]. There is a thickening of the buffer layer causing a turbulent kinetic energy redistribution, increasing in magnitude with viscoelasticity. The cause of this is in part due to a reduction in the pressure-velocity correlation found in the full Reynolds Stress Model [11]. In the context of RANS modelling, Iaccarino [30] attempted to model this effect implicitly by proposing an effective rate of production within the f equation of the $v^2 - f$ model, where f represents the turbulent redistribution process. Direct modelling of this term is complex and can lead to numerical stiffness and complete relaminarisation in previous models [30; 21]. An alternative is to model this effect implicitly with a modified damping function, which can capture the dynamics of the eddy viscosity in viscoelastic flows. Here the constant a_μ in Eq. (20) is enhanced to incorporate an effective thickening of the buffer layer, as similarly presented in [36]. This term is made proportional to the polymer stretching term, C_{kk}/L, which is shown to be proportional to DR in the DNS studies [13]. The term $(1 - A)$ ensures smooth variations in the buffer and logarithmic layer, causing a global reduction in the eddy viscosity as shown in the DNS studies [13].

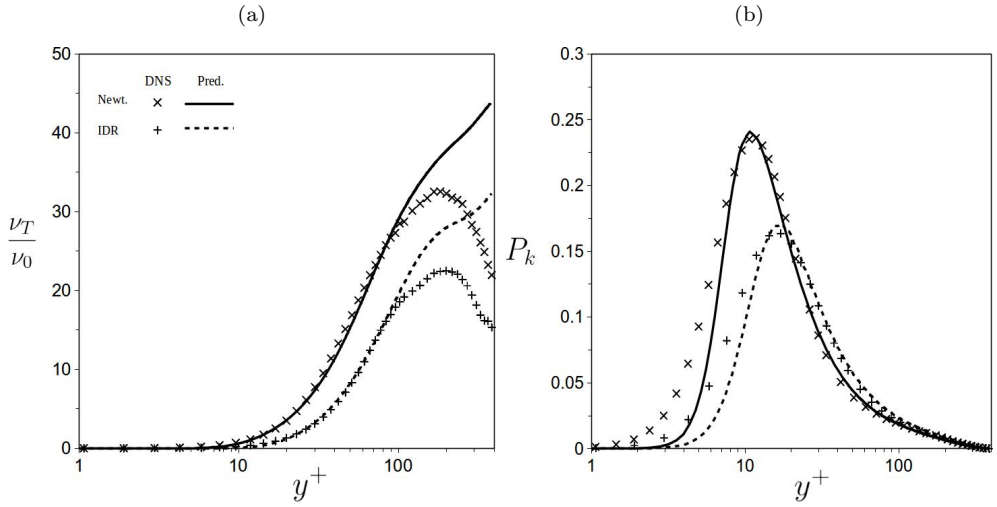

Figure 4: Comparison of the (a) local eddy viscosity and (b) mean production of turbulent kinetic energy between DNS data (symbols) and model predictions (lines) for channel flow at $Re_{\tau_0} = 395$. Newtonian [42] and case 16 (IDR).

The complete modified damping function is presented as,

$$f_\mu = (1 - A)\left[1 - \exp\left(-\frac{y^*}{a_\mu\,(1 + B/a_\mu)}\right)\right]^2, \tag{29}$$

$$A = C_A\left(f_N \frac{\lambda^2}{f(C_{kk})^2}\left(\frac{L}{30}\right)^{3/2}\frac{\varepsilon}{\nu_0}\right)^{0.3}, \tag{30}$$

$$B = C_B(1-\beta)^{0.2}\frac{(C_{kk}-3)^{1.25}}{L}, \tag{31}$$

with y^* given by Eq. (19) and model constants $C_A = 0.071$ and $C_B = 0.69$.

The performance of f_μ is tested against DNS data (case (16), IDR) in fully developed channel flow by analysing the effects on the local eddy viscosity (Fig. 4a). As viscoelasticity is increased, the decrease of the eddy viscosity is

captured well. The thickening of the buffer layer is a result of the high near-wall polymer extension, along with an overall global reduction in the eddy viscosity compared with the Newtonian case, both of which are accurately predicted within the closure model. The effect on the mean production is also shown in Fig. 4b, capturing the peak location and magnitude well. A sensitivity study was performed by varying the f_μ parameters C_A and C_B by $\pm 10\%$ and $\pm 20\%$ (Table 2) with drag reduction as the output. The effect on the mean velocity can be viewed in Fig. 5. The overall change in drag reduction predictions with varying parameters does not substantially change the results, thus confirming the robustness of the closure presented.

C_A	$\mathbf{DR}_A$ (%)	C_B	$\mathbf{DR}_B$ (%)
0.057(-20%)	33.55(-4.8%)	0.62(-20%)	32.31(-8.3%)
0.064(-10%)	34.31(-2.7%)	0.62(-10%)	33.82(-4.1%)
0.071(0%)	35.26(0%)	0.69(0%)	35.26(0%)
0.078(10%)	36.06(2.2%)	0.76(10%)	36.55(3.6%)
0.085(20%)	36.99(4.9%)	0.83(20%)	37.82(7.2%)

Table 2: Sensitivity study of drag reduction value with variations in f_μ parameters C_A and C_B by $\pm 10\%$ and $\pm 20\%$.

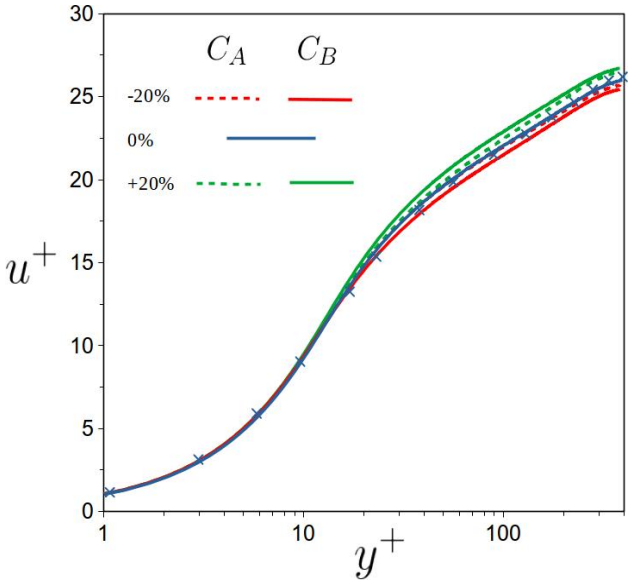

Figure 5: Effect of varying parameters C_A and C_B on the mean velocity profile for IDR (case 16). DNS given by blue cross (×).

4.3. Development of closures within the k and ε transport equations

The viscoelastic closure models required in the k and ε transport equations are ε^V and E_{τ_p}, respectively. The viscoelastic stress work, ε^V, can be expressed as

$$\varepsilon^V = \frac{\nu_p}{\lambda}\left[C_{ij}\overline{f(C_{mm}+c_{mm})\frac{\partial u_i}{\partial x_j}} + \overline{c_{ij}f(C_{mm}+c_{mm})\frac{\partial u_i}{\partial x_j}}\right]. \tag{32}$$

Pinho et al. [22] verified that in LDR, the triple correlation can be decoupled into a double correlation and product of $f(C_{kk})$, which is $NLT_{kk}/2$. Therefore the viscoelastic stress can be approximated by,

$$\varepsilon^V \approx \frac{\nu_\mathrm{p}}{2\lambda} f(C_{mm}) NLT_{mm}. \tag{33}$$

This approximation is well founded and is applied in previous models [15; 33; 36]. Masoudian et al. [15] confirmed the model capabilities within 5% accu-

racy for all DR regimes via an extensive pdf (probability density function) study.

The closure model derived for E_{τ_p} assumes that it depends on the same quantities as the classical Newtonian destruction term of the transport equation of ω, but involving a viscoelastic quantity, typically with the viscoelastic stress work used by Resende et al. [27; 28; 36] and Masoudian et al. [15; 33]. However, the models of Masoudian et al. [15; 33] show an opposite trend in ε for increasing DR, which could be explained by the negative contribution of ε^V in the buffer layer.

The closure derived by Resende et al. [28] in the previous $k-\omega$ is very complex with Wi_{τ_0} dependence to force the correct trend in ε. Here, a much simpler approach is obtained with dependence through k which increases with DR, along with the polymer length and concentration via L and $1-\beta = \nu_p/\nu_0$ respectively. The closure is given by

$$E_{\tau_p} \approx -C_{N4}\frac{\omega}{k}\left[\nu_p\sqrt{C_\mu f_\mu}\left(\frac{L}{30}\right)^{0.65}\left(\frac{k}{\nu_0}\right)^2\right], \tag{34}$$

with model constant $C_{N4} = 0.026$. The effect of Eq. (34) on ε predictions can be viewed in the results section for LDR and HDR.

Overall, it is clear that all the developed viscoelastic closures presented in this study perform well compared with DNS data. Most importantly, this was achieved without the need for extra damping functions or the use of friction velocity dependence. The simplicity of the governing closures allows easy implementation into 3D codes and can be extended to flows with reattachment when DNS data becomes available.

5. Summary of the present model

The governing and transport equations are given below, using the closures developed in the previous section.

Momentum equation:

$$\rho\frac{DU_i}{Dt} = -\frac{\partial\overline{p}}{\partial x_i} + \frac{\partial}{\partial x_k}\left[(\mu_s+\nu_T)\frac{\partial U_i}{\partial x_k}\right] + \frac{\partial}{\partial x_k}\left(\frac{\mu_p}{\lambda}\left[f(C_{kk})C_{ij}-\delta_{ij}\right]\right), \quad (35)$$

where the eddy viscosity is given by

$$\nu_T = f_\mu\frac{k}{\omega}, \quad (36)$$

with modified damping function

$$f_\mu = (1-A)\left[1-\exp\left(-\frac{y^*}{a_\mu\left(1+B/a_\mu\right)}\right)\right]^2, \quad (37)$$

$$A = C_A\left(f_N\frac{\lambda^2}{f(C_{kk})^2}\left(\frac{L}{30}\right)^{3/2}\frac{\varepsilon}{\nu_0}\right)^{0.3}, \quad (38)$$

$$B = C_B(1-\beta)^{0.2}\frac{(C_{kk}-3)^{1.25}}{L}, \quad (39)$$

with constants $a_\mu = 26.5$, $C_A = 0.071$ and $C_B = 0.69$. y^* given by Eq. (19).

Conformation tensor equation:

$$\frac{DC_{ij}}{Dt} - M_{ij} - NLT_{ij} = -\frac{1}{\lambda}[f(C_{kk})C_{ij}-\delta_{ij}], \quad (40)$$

with M_{ij} given by Eq. (12) and

$$\begin{aligned} NLT_{ij} =& f_N C_{N1}C_\mu\frac{\lambda\sqrt{L}k\omega}{\nu_0 f(C_{mm})}\delta_{ij} - f_N^{1/4}C_{N2}M_{ij} \\ &+ C_{N3}\frac{k}{\nu_0}\sqrt{\frac{L(1-\beta)M_{nn}}{\gamma}}\frac{\frac{\partial U_i}{\partial x_k}\frac{\partial U_j}{\partial x_k}}{\gamma^2}, \end{aligned} \quad (41)$$

where $f_N = \nu_T/\nu_0$ is the local eddy viscosity, $\gamma = \sqrt{2S_{pq}S_{pq}}$ is the shear rate invariant, with model constants $C_{N1} = 0.02$, $C_{N2} = 0.3$ and $C_{N3} = 0.18$.

Transport equation of k:

$$\rho\frac{Dk}{Dt} = \frac{\partial}{\partial x_i}\left[\left(\mu_\mathrm{s} + \frac{\rho\nu_\mathrm{T}}{\sigma_k}\right)\frac{\partial k}{\partial x_i}\right] + P_k - C_\mu\rho\omega k - \frac{\nu_p}{\lambda}f(C_{mm})\frac{NLT_{mm}}{2}. \tag{42}$$

Specific rate of dissipation transport equation:

$$\rho\frac{D\omega}{Dt} = \frac{\partial}{\partial x_i}\left[\left(\mu_\mathrm{s} + \frac{\rho\nu_\mathrm{T}}{\sigma_\omega}\right)\frac{\partial \omega}{\partial x_i}\right] + \frac{C_\omega}{k}(\mu_s + \nu_T)\frac{\partial k}{\partial x_i}\frac{\partial \omega}{\partial x_i} + \frac{\omega}{k}\left(C_{\omega_1}P_k - C_{N4}\nu_p\sqrt{C_\mu f_\mu}\left(\frac{L}{30}\right)^{0.65}\left(\frac{k}{\nu_0}\right)^2\right) - C_{\omega_2}\rho\omega^2 \tag{43}$$

and model constant $C_{N4} = 0.026$.

The remaining constant are of the Newtonian model and are $C_\omega = 0.9$, $C_{\omega_1} = 0.49$, $C_{\omega_2} = 0.072$, $C_\mu = 0.09$, $\sigma_k = 1.0$ and $\sigma_\omega = 1.8$.

6. Results and discussion

In order to examine the viscoelastic turbulence model against the available DNS data identified within the literature, a new finite volume C++ computational solver was developed in the OpenFOAM software. A fully-developed channel flow using half of the channel height, h, is applied given the symmetry of the governing geometry. 100 cells are assigned in the transverse (y-direction) with approximately 10 cells located inside the viscous sublayer. This is to provide mesh independent results, with errors within 0.5% for the

mean velocity and the friction factor compared with a very fine mesh as reported in [33]. To improve numerical stability, an artificial diffusion term is added to the RACE in the form, $\kappa\partial_k^2 C_{ij}$, where κ denotes a constant, isotropic, artificial numerical diffusivity. In earlier studies [33], the dimensionless artificial numerical diffusivity is taken to be $\kappa/hu_\tau \sim O(10^{-3})$ and is also implemented here. The diffusion has a negligible impact on overall DR predictions. No-slip boundary conditions are imposed on the solid wall for the velocity field U, along with $k = 0$. The specific rate of dissipation, ω, follows the asymptotic formed by Wilcox [45] such that, $\omega \to \frac{2\nu_s}{C_\mu y^2}$ as $y \to 0$. A Dirichlet boundary condition for C_{ij} is applied as reported in [39].

The model performance is assessed against a range of different flow and rheological parameters presented in the DNS data within Table 1.

Fig. 6 plots the components of the conformation tensor (C_{zz} excluded) and shows good agreement with the DNS data for LDR and HDR. The C_{xx} component is dominated by NLT_{xx}, the new term modelled. The peak location near the wall and decay towards the centre is well captured (Fig. 6a). The shear component C_{xy} (Fig. 6c) has most effect on the flow in a region $y^+ < 50$ according to the findings of Li et al. [13], which is captured here for LDR and HDR. Finally the C_{yy} component is shown in Fig. 6b, which is important for an effective polymer viscosity, shown here to capture the shift away from the wall for increasing DR.

Fig. 7 shows the turbulent kinetic energy profiles for Newtonian and IDR. The increase of k and peak location is captured well, improving greatly upon previous model predictions. Fig. 8 demonstrates the model capabilities of predicting low and high DR.

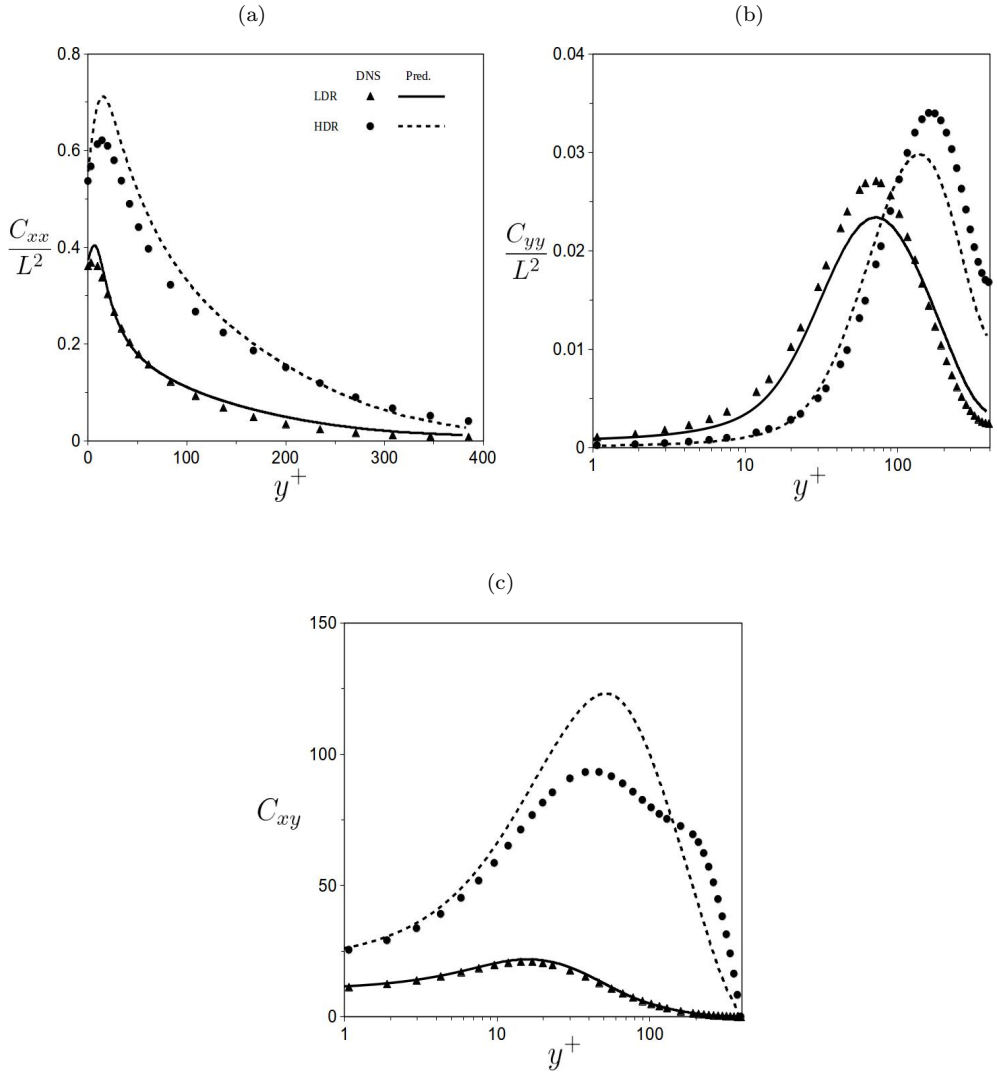

Figure 6: Comparison of the conformation tensor components between DNS data (symbols) and model predictions (lines) for channel flow at $Re_{\tau_0} = 395$: (a) C_{xx}/L^2 (legend used for all figures); (b) C_{yy}/L^2; (c) C_{xy}. case 13 (LDR) and case 17 (HDR).

The Newtonian dissipation of k is plotted in Fig. 9 and shows good agreement with DNS for LDR and HDR. The near-wall values lose accuracy

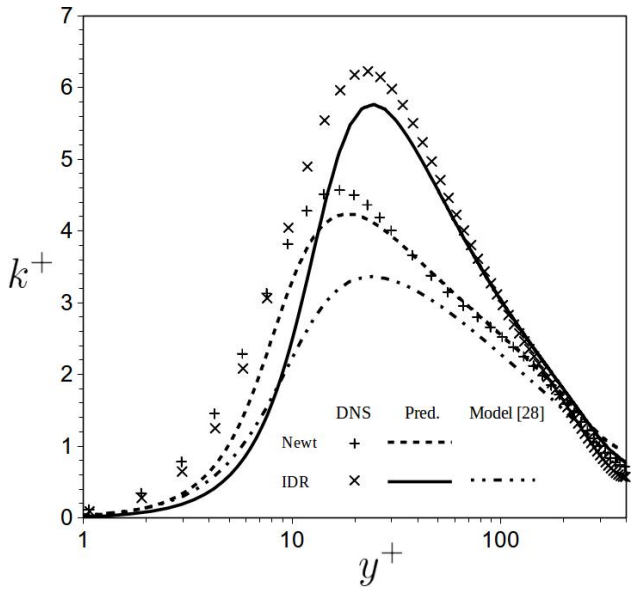

Figure 7: Comparison of the turbulent kinetic energy, k, between DNS data (symbols) and model predictions (lines) for channel flow at $Re_{\tau_0} = 395$. Newtonian [42], case 16 (IDR).

which is a known defect in isotropic $k-\varepsilon$ models. The closure for E_{τ_p} predicts well the decrease in ε as viscoelasticity increases.

The local eddy viscosity is plotted in Fig. 10 for all ranges of DR at $Re_{\tau_0} = 395$. The decrease of ν_T with increasing viscoelasticity is predicted well, capturing the thickening of the buffer layer and reduction in the log-layer ascertained by the modified damping function.

The overall stress balance is plotted in Fig. 11a, with the Reynolds stress, solvent stress and polymer stress. Good predictions of the stress balance determines the velocity profile accuracy. The mean stream-wise velocity profiles for all ranges of DR at $Re_{\tau_0} = 395$ are plotted in Fig. 11b. The maximum drag reduction asymptote of Virk [2] is also plotted here, along with the viscous sub-layer and log law equations. The model can predict well the increase

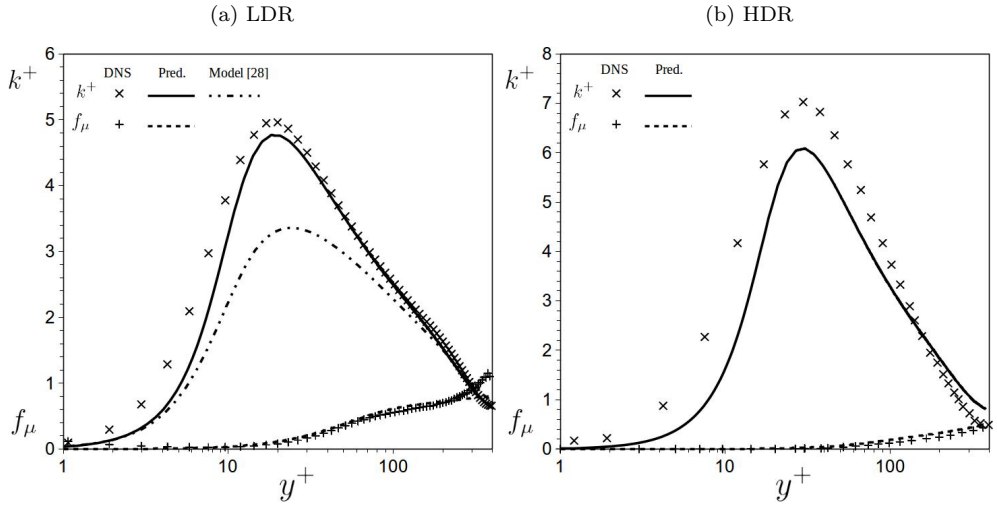

Figure 8: Comparison of the turbulent kinetic energy, k, and damping function, f_μ, between DNS data (symbols) and model predictions (lines) for channel flow at $Re_{\tau_0} = 395$: (a) case 13 (LDR); (b) case 17 (HDR).

in the log law for increasing DR. At LDR the model over-predicts, but has an improved performance at different Reynolds numbers. For MDR there is an under-prediction due to the limitations of the isotropic assumptions, where the near-wall eddies become excessively dampened, but still captures fairly well the overall increase of the log law profile. Fig. 12 shows the model capability in predicting a range of Reynolds numbers and flow parameters. This is extended with small β variation as shown in Fig. 13 which shows good agreement with the DNS data.

Overall it is evident that the model can predict drag reducing features well for a range of flow and rheological parameters, where the main advantage is through model simplicity and without friction velocity dependence compared

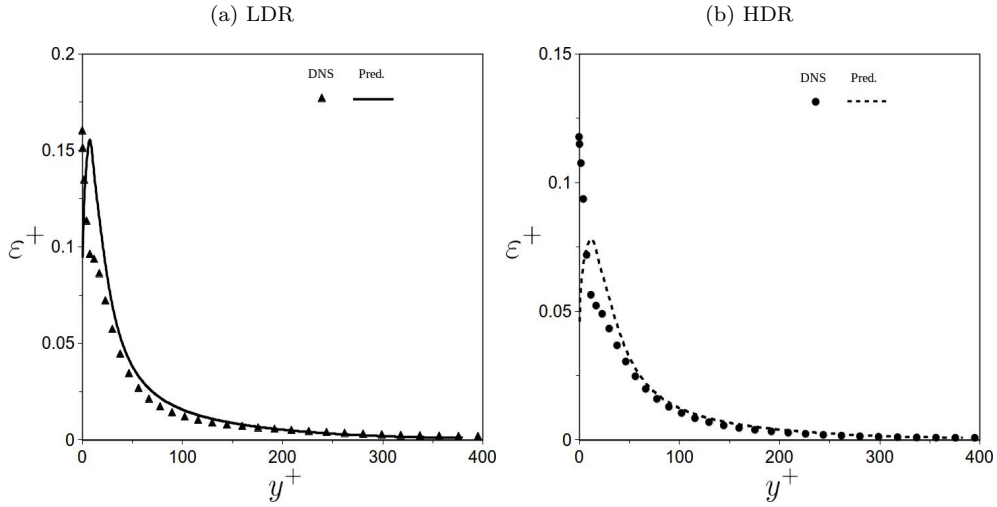

Figure 9: Comparison of the true Newtonian dissipation rate of k between DNS data (symbols) and model predictions (lines) for channel flow at $Re_{\tau_0} = 395$: (a) case 13 (LDR); (b) case 17 (HDR).

to the previous isotopic models [27; 28; 36].

7. Conclusions

A viscoelastic turbulence model in fully-developed drag reducing channel flow is improved, with turbulent eddies modelled under a $k - \omega$ representation, along with polymeric solutions described by the finitely extensible nonlinear elastic-Peterlin (FENE-P) constitutive model. The Newtonian model of Bredberg [29] is modified to include a new Van-Driest type damping function but including a near-wall scaling, y^*, such that $y^+ \sim y^*$ for $y^+ < 100$. The model performance is evaluated against a variety of rheological parameters within the DNS data literature including: friction Reynolds number $Re_{\tau_0} = 125, 180, 300, 395, 590$; Wiessenberg number

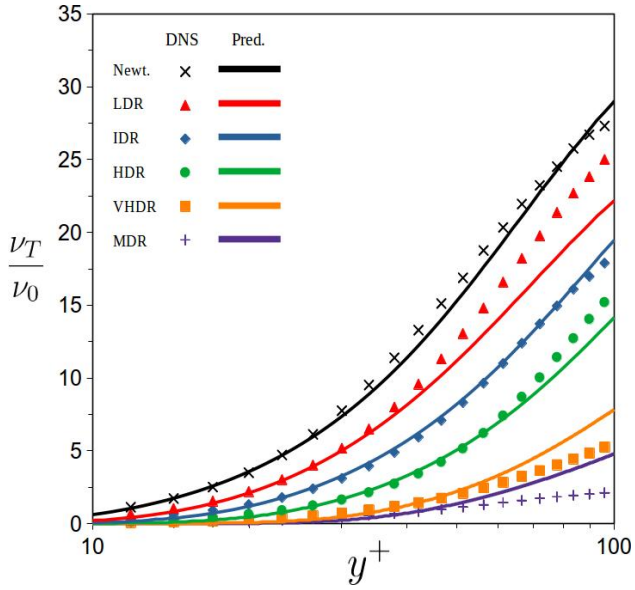

Figure 10: Comparison of the local eddy viscosity between DNS data (symbols) and model predictions (lines) for channel flow at $Re_{\tau_0} = 395$. Each colour represents a different drag reduction regime: Newtonian [42]; case 13 (LDR); case 16 (IDR); case 17 (HDR); case 19 (Very HDR); case 21 (MDR).

$Wi_{\tau_0} = 25, 36, 50, 54, 72, 100, 116, 200$; polymer concentration $\beta = 0.9, 0.8, 0.6$; and maximum molecular extensibility of the dumbbell chain $L^2 = 900, 1000, 1800, 3600, 10000, 14400$. The DNS data for $Re_{\tau_0} = 395$ in Table 1 is used for the calibration of the closures developed for the turbulent cross correlations identified in section 4. The model is capable of predicting a large range of flow features for low and high Reynolds number at all regimes of DR and improves significantly on the model of Resende et al. [28], with its ability to capture higher Reynolds numbers with simpler closures.

The main feature is the modified damping function, f_μ, which is capable of predicting the reduction in the eddy viscosity and effective thickening

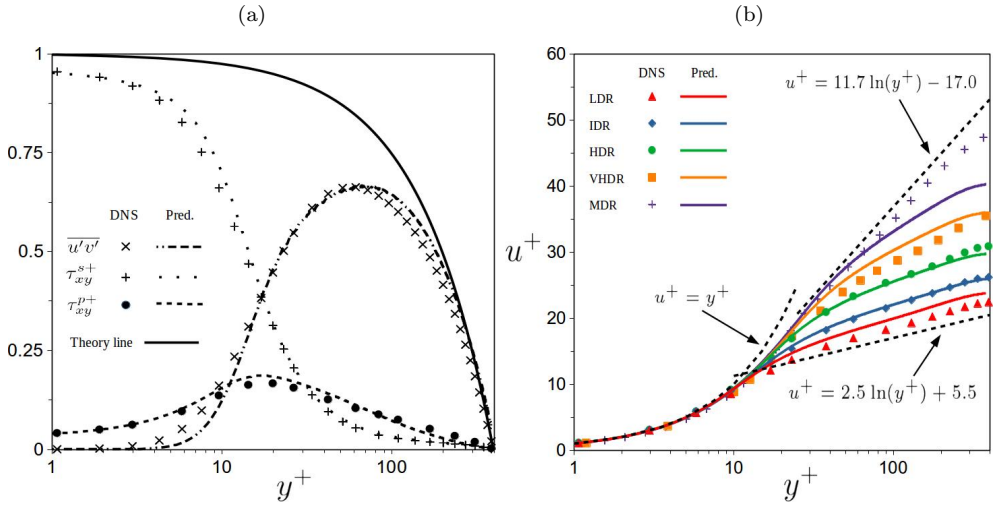

Figure 11: Comparison of (a) normalised shear stresses (case 16 (IDR)) and (b) mean stream-wise velocity profiles between DNS data (symbols) and model predictions (lines) for channel flow at $Re_{\tau_0} = 395$. Each colour represents a different drag reduction regime: case 13 (LDR); case 16 (IDR); case 17 (HDR); case 19 (Very HDR); case 21 (MDR). The viscous sub-layer equation, log layer equation, and Virk's asymptote [2] are also shown (dotted lines) in (b).

of the buffer layer as viscoelasticity increases. The correct increase in the turbulent kinetic energy, k, is also shown and improves greatly on the previous model [28]. The model can also capture small β variation in accordance with the FENE-P limits, highlighted with the dependence on $1-\beta$, which is proportional to the polymer concentration. Further improvements are developed within the closures of the NLT_{ij} and E_{τ_p} terms present within the governing equations after the Reynolds averaging process. The NLT_{ij} model presents a better performance for all regimes of DR when compared with the previous $k-\omega$ model [28]. The main advantage of the closure is the reduc-

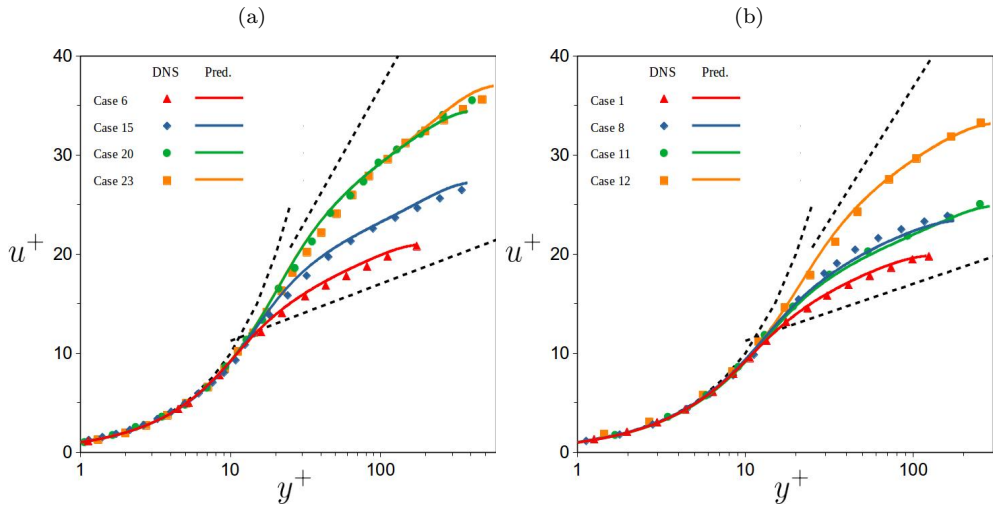

Figure 12: Comparison of the mean stream-wise velocity profiles between DNS data (symbols) and model predictions (lines) for channel flow at various Reynolds numbers. Each colour represents a different case. See Fig. 11b for dotted lines.

tion in the complexity and damping functions in the dominant contribution, NLT_{xx}, modelled here to increase with turbulent kinetic energy as the flow viscoelasticity increases. In terms of the viscoelastic destruction term, E_{τ_p}, previous isotropic models developed by Resende et al. [27; 28; 36] required friction velocity dependence which is here removed and greatly simplifies the model, keeping the same prediction accuracy of ε.

Overall, the model predicts very well across a wide range of DNS data and significantly improves on capturing all flow features with simplicity and performance compared with the most recent $k-\omega$ model developed by Resende et al. [28], which was limited to a few DNS data cases. The current model extends on the recently developed $k-\varepsilon$ model [39], but here including β variation up-to the FENE-P limits, and with a Newtonian model based on

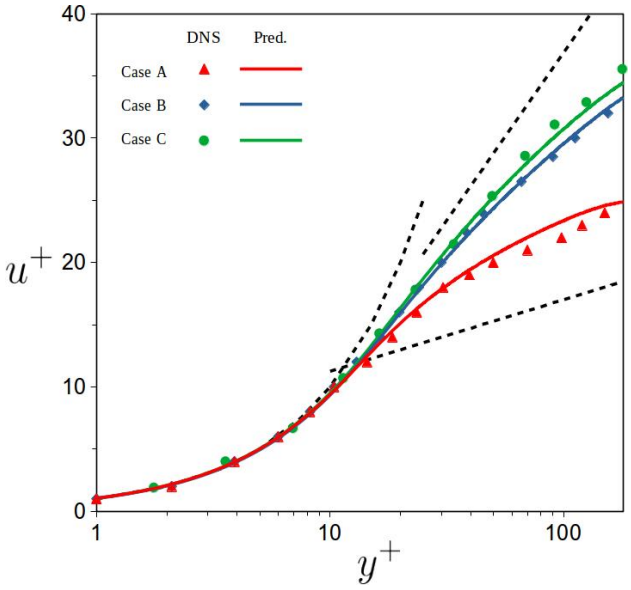

Figure 13: Comparison of the mean stream-wise velocity profiles between DNS data (symbols) and model predictions (lines) for channel flow at varying β at $Re_{\tau_0} = 180$. Each colour represents a different case. See Fig. 11b for dotted lines.

$k - \omega$ that is naturally more numerically stable and is designed for predictions in complex flow such as the Backward-facing step. The simplicity of the present model allows easy implementation into 3D codes and increases numerical stability. All friction velocity dependence is removed in the present model which is the first of its kind for isotropic models with damping functions, whose main advantage is the development of simulations in geometries with reattachment.

Acknowledgement

Financial support for this studentship project from the Engineering and Physical Sciences Research Council (EPSRC) [Grant number: EP/N5059681/1,

Award Reference: 1958044] is greatly acknowledged by M. McDermott.

References

[1] B. A. Toms, Some observations on the flow of linear polymer solutions through straight tubes at large reynolds numbers, Proc. of In. Cong. On Rheology, 1948 135 (1948).

[2] P. S. Virk, E. Merrill, H. Mickley, K. Smith, E. Mollo-Christensen, The toms phenomenon: turbulent pipe flow of dilute polymer solutions, Journal of Fluid Mechanics 30 (2) (1967) 305–328.

[3] J. L. Lumley, Drag reduction by additives, Annual review of fluid mechanics 1 (1) (1969) 367–384.

[4] M. Tabor, P. De Gennes, A cascade theory of drag reduction, EPL (Europhysics Letters) 2 (7) (1986) 519.

[5] V. S. L'vov, A. Pomyalov, I. Procaccia, V. Tiberkevich, Drag reduction by polymers in wall bounded turbulence, Physical review letters 92 (24) (2004) 244503.

[6] T. Min, J. Y. Yoo, H. Choi, D. D. Joseph, Drag reduction by polymer additives in a turbulent channel flow, Journal of Fluid Mechanics 486 (2003) 213–238.

[7] V. Dallas, J. C. Vassilicos, G. F. Hewitt, Strong polymer-turbulence interactions in viscoelastic turbulent channel flow, Physical Review E 82 (6) (2010) 066303.

[8] L. Thais, T. B. Gatski, G. Mompean, Analysis of polymer drag reduction mechanisms from energy budgets, International Journal of Heat and Fluid Flow 43 (2013) 52–61.

[9] R. Bird, P. Dotson, N. Johnson, Polymer solution rheology based on a finitely extensible bead—spring chain model, Journal of Non-Newtonian Fluid Mechanics 7 (2-3) (1980) 213–235.

[10] R. B. Bird, R. C. Armstrong, O. Hassager, Dynamics of polymeric liquids. vol. 1: Fluid mechanics, N/A (1987).

[11] Y. Dubief, G. Laccarino, S. Lele, A turbulence model for polymer flows, Center for Turbulence Research, Stanford (2004).

[12] R. Sureshkumar, A. N. Beris, R. A. Handler, Direct numerical simulation of the turbulent channel flow of a polymer solution, Physics of Fluids 9 (3) (1997) 743–755.

[13] C.-F. Li, R. Sureshkumar, B. Khomami, Influence of rheological parameters on polymer induced turbulent drag reduction, Journal of Non-Newtonian Fluid Mechanics 140 (1-3) (2006) 23–40.

[14] P. Ptasinski, B. Boersma, F. Nieuwstadt, M. Hulsen, B. Van den Brule, J. Hunt, Turbulent channel flow near maximum drag reduction: simulations, experiments and mechanisms, Journal of Fluid Mechanics 490 (2003) 251–291.

[15] M. Masoudian, K. Kim, F. Pinho, R. Sureshkumar, A viscoelastic k-ε-v2-f turbulent flow model valid up to the maximum drag reduction limit, Journal of Non-Newtonian Fluid Mechanics 202 (2013) 99–111.

[16] F. Pinho, A gnf framework for turbulent flow models of drag reducing fluids and proposal for ak–ε type closure, Journal of Non-Newtonian Fluid Mechanics 114 (2-3) (2003) 149–184.

[17] D. Cruz, F. Pinho, Turbulent pipe flow predictions with a low reynolds number k–ε model for drag reducing fluids, Journal of Non-Newtonian Fluid Mechanics 114 (2-3) (2003) 109–148.

[18] D. Cruz, F. Pinho, P. Resende, Modelling the new stress for improved drag reduction predictions of viscoelastic pipe flow, Journal of non-newtonian fluid mechanics 121 (2-3) (2004) 127–141.

[19] P. Resende, M. Escudier, F. Presti, F. Pinho, D. Cruz, Numerical predictions and measurements of reynolds normal stresses in turbulent pipe flow of polymers, International Journal of Heat and Fluid Flow 27 (2) (2006) 204–219.

[20] P. Resende, F. Pinho, D. Cruz, A reynolds stress model for turbulent flows of viscoelastic fluids, Journal of Turbulence 14 (12) (2013) 1–36.

[21] R. Leighton, D. T. Walker, T. Stephens, G. Garwood, Reynolds stress modeling for drag reducing viscoelastic flows, in: ASME/JSME 2003 4th Joint Fluids Summer Engineering Conference, American Society of Mechanical Engineers, 2003, pp. 735–744.

[22] F. Pinho, C. Li, B. Younis, R. Sureshkumar, A low reynolds number turbulence closure for viscoelastic fluids, Journal of Non-Newtonian Fluid Mechanics 154 (2-3) (2008) 89–108.

[23] Y. Nagano, M. Hishida, Improved form of the k-ε model for wall turbulent shear flows, Journal of fluids engineering 109 (2) (1987) 156–160.

[24] Y. Nagano, Modeling the dissipation-rate equation for two-equation turbulence model, in: Proc. 9th Symp. on Turbulent Shear Flows, 1993, pp. 23–2.

[25] K. D. Housiadas, A. N. Beris, R. A. Handler, Viscoelastic effects on higher order statistics and on coherent structures in turbulent channel flow, Physics of Fluids 17 (3) (2005) 035106.

[26] C. Li, V. Gupta, R. Sureshkumar, B. Khomami, Turbulent channel flow of dilute polymeric solutions: drag reduction scaling and an eddy viscosity model, Journal of Non-Newtonian Fluid Mechanics 139 (3) (2006) 177–189.

[27] P. Resende, K. Kim, B. Younis, R. Sureshkumar, F. Pinho, A fene-p k–ε turbulence model for low and intermediate regimes of polymer-induced drag reduction, Journal of Non-Newtonian Fluid Mechanics 166 (12-13) (2011) 639–660.

[28] P. Resende, F. Pinho, B. Younis, K. Kim, R. Sureshkumar, Development of a low-reynolds-number k-ω model for fene-p fluids, Flow, turbulence and combustion 90 (1) (2013) 69–94.

[29] J. Bredberg, S.-H. Peng, L. Davidson, An improved k- ω turbulence model applied to recirculating flows, International journal of heat and fluid flow 23 (6) (2002) 731–743.

[30] G. Iaccarino, E. S. Shaqfeh, Y. Dubief, Reynolds-averaged modeling of polymer drag reduction in turbulent flows, Journal of Non-Newtonian Fluid Mechanics 165 (7-8) (2010) 376–384.

[31] P. A. Durbin, Separated flow computations with the k-epsilon-v-squared model, AIAA journal 33 (4) (1995) 659–664.

[32] R. Benzi, A short review on drag reduction by polymers in wall bounded turbulence, Physica D: Nonlinear Phenomena 239 (14) (2010) 1338–1345.

[33] M. Masoudian, F. Pinho, K. Kim, R. Sureshkumar, A rans model for heat transfer reduction in viscoelastic turbulent flow, International Journal of Heat and Mass Transfer 100 (2016) 332–346.

[34] M. Masoudian, K. Kim, F. Pinho, R. Sureshkumar, A reynolds stress model for turbulent flow of homogeneous polymer solutions, International Journal of Heat and Fluid Flow 54 (2015) 220–235.

[35] Y. Lai, R. So, On near-wall turbulent flow modelling, Journal of Fluid Mechanics 221 (1990) 641–673.

[36] P. Resende, A. Afonso, D. Cruz, An improved k-ε turbulence model for fene-p fluids capable to reach high drag reduction regime, International Journal of Heat and Fluid Flow 73 (2018) 30–41.

[37] P. Resende, F. Pinho, P. Oliveira, Improvement of the energy distribution in isotropic turbulent viscoelastic fluid models, MEFTE 2014 (2014) 221.

[38] P. Resende, A. Cavadas, New developments in isotropic turbulent models for fene-p fluids, Fluid Dynamics Research 50 (2) (2018) 025508.

[39] M. McDermott, P. Resende, T. Charpentier, M. Wilson, A. Afonso, D. Harbottle, G. d. Boer, A fene-p k-ε viscoelastic turbulence model valid up to high drag reduction without friction velocity dependence, Applied Sciences 10 (22) (2020) 8140.

[40] T. Tsukahara, Y. Kawaguchi, Proposal of damping function for low-reynolds-number-model applicable in prediction of turbulent viscoelastic-fluid flow, Journal of Applied Mathematics 2013 (2013).

[41] S. Wallin, A. V. Johansson, An explicit algebraic reynolds stress model for incompressible and compressible turbulent flows, Journal of Fluid Mechanics 403 (2000) 89–132.

[42] R. D. Moser, J. Kim, N. N. Mansour, Direct numerical simulation of turbulent channel flow up to retau590, Physics of fluids 11 (4) (1999) 943–945.

[43] L. Thais, T. B. Gatski, G. Mompean, Some dynamical features of the turbulent flow of a viscoelastic fluid for reduced drag, Journal of Turbulence 13 (19) (2012) N19.

[44] M. Masoudian, C. da Silva, F. Pinho, Grid and subgrid-scale interactions in viscoelastic turbulent flow and implications for modelling, Journal of Turbulence 17 (6) (2016) 543–571.

[45] D. C. Wilcox, Turbulence modeling, DCW Industries (1993).